Sum and difference frequency generation as diagnostics for leaky eigenmodes in two-dimensional photonic crystal waveguides

A. D. Bristow, J. P. Mondia,[a] and H. M. van Driel[b]
Department of Physics & Institute for Optical Sciences, University of Toronto, Toronto, Ontario M5S 1A7, Canada

(Received 3 June 2005; accepted 30 November 2005; published online 31 January 2006)

We experimentally demonstrate how sum frequency generation (SFG) and difference frequency generation (DFG) of 150 fs pulses can be enhanced and serve as diagnostics for leaky eigenmodes in a two-dimensional GaAs photonic crystal waveguide. SFG at 795 nm is obtained in reflection from *s*-polarized 1900 nm and *p*-polarized 1360 nm pulses, with both input beams coupled to leaky eigenmodes; the SFG is enhanced by $>350\times$ compared to that from an untextured GaAs surface. We are able to detect Drude induced subnanometer blueshifts of the SFG, corresponding to refractive index changes of $\leqslant 10^{-3}$. DFG of 1360 nm light obtained in reflection from *s*-polarized 1900 nm and *p*-polarized 793 nm pulses displays an enhancement of $>500\times$ via three different leaky eigenmodes. As the 793 nm beam polarization is varied from *p* polarized to right and left circularly polarized, the DFG remains essentially linearly polarized but with a reduced, albeit different, intensity for right and left circularly polarized 795 nm pulses. Futhermore, the plane of polarization also rotates by different amounts for the left and right circularly polarized light, demonstrating interference of the components generated by *s*- and *p*-polarized 793 nm pulses. Overall, our results demonstrate how enhanced DFG and SFG from leaky eigenmodes can be used to characterize their properties more precisely than linear optical techniques. © *2006 American Institute of Physics*. [DOI: 10.1063/1.2161415]

I. INTRODUCTION

Two-dimensional (2D) arrays of air holes patterned into planar waveguides, otherwise known as photonic crystal waveguides (PCWs), can provide an innovative control of electromagnetic radiation in three dimensions.[1] While the optical properties of these structures are sometimes difficult to discern via linear optical techniques, recently it has been shown that enhancement of second-harmonic generation can serve as a better diagnostic tool.[2–5] When a fundamental optical beam is incident on these structures, for certain angles of incidence and polarization either the fundamental or the second-harmonic beam can couple to a leaky eigenmode (LEM), resulting in enhanced harmonic generation with sharp spectral features, particularly if the modes have a reasonable quality (Q) factor. By comparison, in experiments where reflectivity is used to probe LEMs, the result[6,7] is broad Fano-like features[8] which are much harder to interpret. Being a degenerate process, second-harmonic generation, however, has limitations as a diagnostic tool since only one wavelength can be varied; further limitations relate to beam polarization and sample absorption characteristics at pump or second-harmonic wavelengths. Similar considerations apply to third-harmonic generation, which can be used to explore short-wavelength features.[9] Nevertheless, additional flexibility for nonlinear techniques can be obtained by exploiting the new degrees of freedom offered by nondegenerate processes and/or noncollinear geometries. In this paper we report the experimental results of sum frequency generation (SFG) and difference frequency generation (DFG) from a $GaAs/Al_2O_3$ PCW in a reflection geometry and illustrate how these processes provide a sophisticated method for investigating LEMs.

SFG and DFG involving three beams are conventionally discussed in terms of a pump, a signal, and an idler beam (with frequencies and wave vectors) characteristically written as $(\omega_p, \mathbf{k}_p)$, $(\omega_s, \mathbf{k}_s)$, and $(\omega_i, \mathbf{k}_i)$ with $\omega_i + \omega_s = \omega_p$. Sum frequency generation is governed by a second-order susceptibility tensor $\chi^{(2)}(-\omega_p; \omega_i, \omega_s)$, while difference frequency generation at ω_s is governed by $\chi^{(2)}(-\omega_s; -\omega_i, \omega_p)$; for bulk GaAs the only nonzero element is $\chi^{(2)}_{xyz}$ and those based on permutations of the orthogonal axes x, y, and z. In bulk crystals the strength of the conversion process is optimal under the phase-matching condition, $\Delta\mathbf{k} = \mathbf{k}_p - \mathbf{k}_s - \mathbf{k}_i = 0$. This cannot be satisfied in bulk GaAs due to normal dispersion and cubic symmetry. However, the translational symmetry of a photonic crystal relaxes the phase-matching condition[2,10] so that $\Delta\mathbf{k} = \mathbf{k}_p - \mathbf{k}_s - \mathbf{k}_i + \mathbf{G}$ might be close to zero for some reciprocal-lattice vector, $\mathbf{G}$.

Furthermore, depending on the symmetry and orientation of the photonic crystal relative to the electronic lattice, additional $\chi^{(2)}$ tensor elements are possible. Even though SFG and DFG can be enhanced by resonant coupling to LEMs under phase-matching conditions, for the beam reflection geometry we employ the overall conversion efficiency is still much smaller (typically $\leqslant 1\%$) than that expected from transmission geometries in which the interaction length is much longer.

The remainder of the paper is organized as follows:

[a]Present address: Max-Planck-Research-Group for Optics, Information and Photonics, Universität Erlangen-Nürnberg, D-91058 Erlangen, Germany.
[b]Electronic mail: vandriel@physics.utoronto.ca

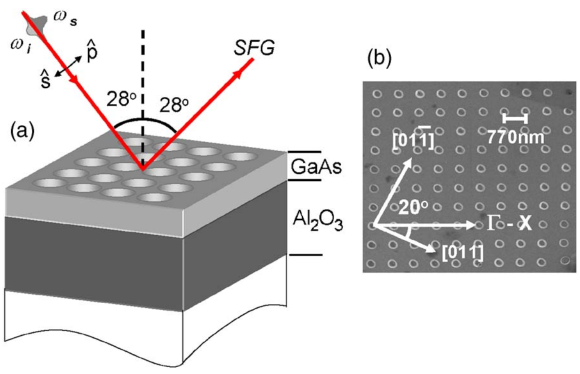

FIG. 1. (Color online) (a) Schematic diagram of the photonic crystal waveguide structure, with the beam geometry shown for SFG. (b) Surface-view scanning electron micrograph of the square photonic lattice with the electronic crystallographic directions [011] and [01$\bar{1}$] indicated.

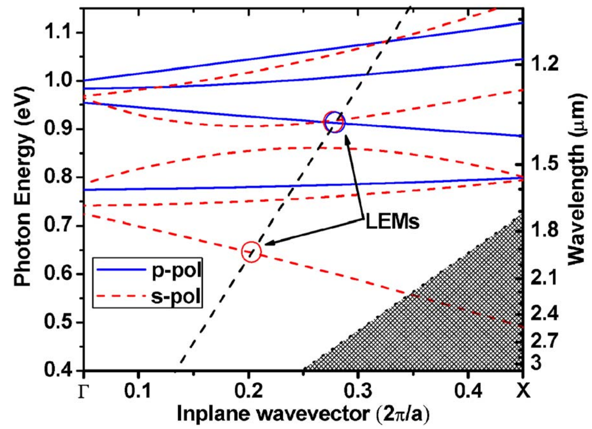

FIG. 2. (Color online) The photonic band structure along the Γ-X high-symmetry direction for both s and p polarizations. The dashed diagonal line represents light incident at 28°. Those circled are the 1360 and 1900 nm photonic eigenmodes that are utilized in both SFG and DFG experiments. The shaded region is inaccessible via surface coupling.

Firstly, a short description of the sample and the experimental technique is given. Secondly, SFG results from experiments using different pulse fluences are presented and yield information about material absorption, LEM tuning, and the Q of the LEMs. Next, results from DFG experiments are reported for both fluence and polarization dependence at an output wavelength corresponding to two orthogonally polarized LEMs illustrating the degree of LEM tuning and narrowing of the DFG spectrum via phase-matching. Finally, we show how the polarization of the DFG emission is sensitive to the polarization of the input beams and how interference effects can be used to identify weak emission processes.

II. EXPERIMENTAL DETAILS

A schematic diagram of the asymmetric waveguide sample is shown in Fig. 1(a). It consists of a 140 nm GaAs core layer on top of a 1-μm-thick Al_2O_3 lower cladding layer grown on a [100] GaAs substrate; air serves as the upper cladding layer. The photonic crystal was patterned by electron-beam lithography and reactive ion etching. It consists of a square lattice of air holes with a 160 nm radius and a 770 nm lattice period, as shown in the scanning electron micrograph in Fig. 1(b). The sample specifications were based on Cowan and Young's[2] design to enhance a p-polarized second-harmonic beam generated in reflection from an incident s-polarized fundamental beam, as confirmed by Mondia *et al.*[5] Because of the symmetry of the $\chi^{(2)}$ tensor, if the Γ-X direction of the photonic crystal lies in the plane of incidence, one requires the electronic and photonic crystal lattices to be misaligned; for our sample the Γ-X direction makes an angle of 20° with respect to the [011] GaAs crystal direction.

Figure 2 shows a portion of the photonic band structure diagram for s- and p-polarized light propagating in the Γ-X crystal direction. The shaded area lies beneath the light line and photonic modes in this region are inaccessible by surface coupling. Above this line are the accessible LEMs. The dashed diagonal line represents light incident at 28° (measured with respect to the normal) for which coupling to certain LEMs is possible. Circled are three LEMs which intersect that line and are the focus of this paper; one LEM occurs at 1900 nm and two LEMs, with orthogonal polarization states, exist at 1360 nm. Not shown is the high-frequency region where SFG yields 795 nm or DFG requires 795 nm. Above the 870 nm electronic band gap of GaAs, such modes would have complex eigenfrequencies, since the absorption length for 795 nm light in bulk GaAs being ~750 nm.[11]

The SFG and DFG experiments were performed with a Ti:sapphire mode-locked oscillator/amplifier system which pumped an optical parametric generator. The latter produced pulses in the 1200–2000 nm wavelength range with pulse widths of 150 fs at a repetition rate of 250 kHz. The pump-laser wavelength was set to 793 nm, corresponding to ω_p for the experiments reported here, and signal and idler pulses were obtained from the parametric generator at 1360 and 1900 nm corresponding to ω_s and ω_i, respectively; the spectral widths of the pulses were determined to be 7.5, 24, and 60 nm, respectively. The various beams were spatially filtered, polarization controlled, and brought collinearly to the sample. Each beam was focused to a $1/e$ spot diameter of 60 μm on the 90×90 μm^2 sample area. For the SFG experiments p-polarized ω_s and s-polarized ω_i pulses were incident with p-polarized SFG light observed to be centered at 795 nm, near ω_p, whereas for the DFG experiment ω_p and ω_i pulses of different polarizations were incident with down-converted light observed near ω_s. In both cases, the ω_s and ω_i beams are both coupled to LEMs creating a double-resonance condition in the PCW. A delay stage in one of the beam paths was used to temporally overlap the pump pulses at the sample. All beams were incident on the sample at 28° with respect to the normal with the Γ-X direction of the photonic crystal being in the plane of incidence. The emission from the photonic crystal was collected along the specularly reflected direction, as shown in Fig. 1(a). The light was passed through a linear polarizer and coupled into a spectrometer. At the exit slits of the spectrometer SFG light was detected by a photomultiplier tube and DFG light by a LN_2-cooled InGaAs photodiode. A double-chopping scheme was used to isolate the parametric generation process, removing any leakage of radiation from the extraneous third beam.

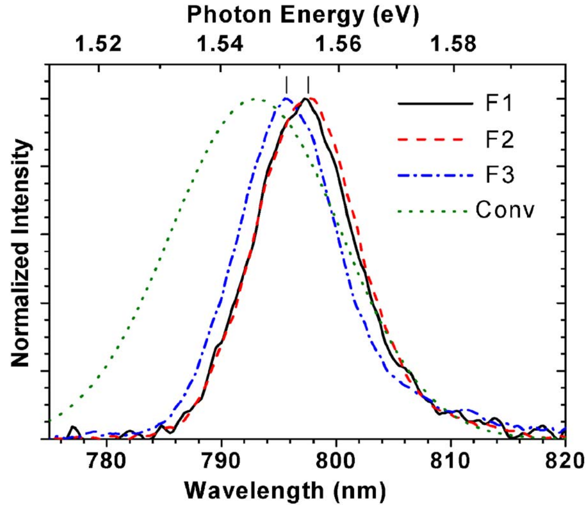

FIG. 3. (Color online) Normalized SFG spectra obtained from the photonic crystal waveguide: For F1 both incident pulses have an 80 μJ cm^{-2} fluence; for F2 the 1360 nm pulse has an 80 μJ cm^{-2} fluence and the 1900 nm beam fluence is 400 μJ cm^{-2}; for F3 the fluences of the two pulses are the reverse of those for F2. The dotted curve is the convolution of the ω_s and ω_i pulses.

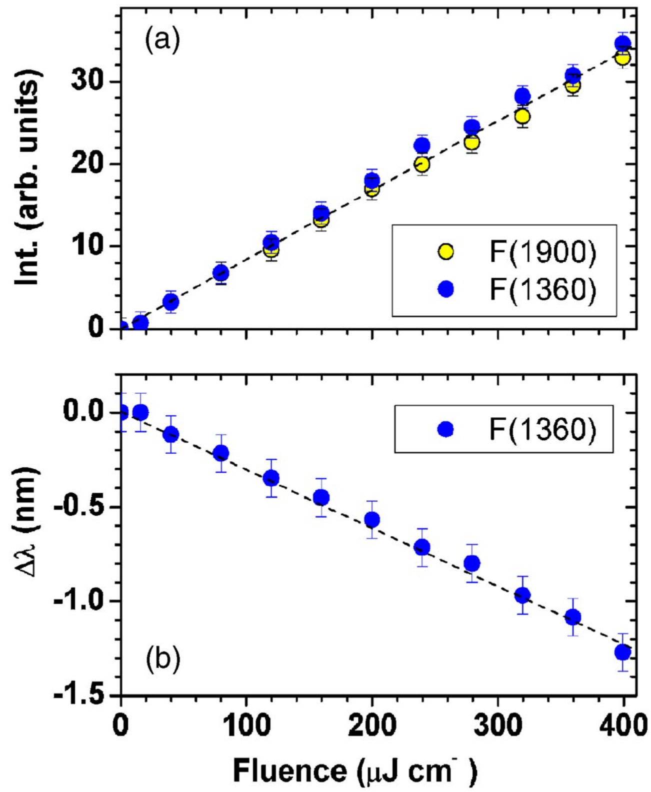

FIG. 4. (Color online) (a) The fluence-dependent SFG amplitude for fixed 1360 nm pulse fluence with variable 1900 nm pulse fluence [F(1900), light circles] and vice versa [F(1360), dark circles]. (b) Wavelength dependence of the SFG peak for the F(1360) case.

The bandwidth of the generated emission is related to the input pulse bandwidths and the Q of the LEMs. The bandwidths from DFG and SFG processes from an external bulk source provide a comparison for the bandwidths of the parametric processes in the PCW. For this, a flipper mirror was placed before the sample directing the beams to a β-barium borate (BBO) crystal used under non-phase-matched conditions; the converted light was then coupled into the spectrometer. Unlike the PCW, the BBO crystal is >3 mm in diameter and parametric generation is not position sensitive; the crystal was therefore useful for system alignment and pulse diagnostics.

III. SUM FREQUENCY GENERATION

For the SFG process the choice of p polarization for the ω_s beam and s polarization for the ω_i beam maximizes the amplitude of the ω_p light so that the spectral and fluence-dependent characteristics can be determined. The ω_i beam couples to an s-polarized LEM, whereas at ω_s two orthogonally polarized LEMs exist. For s-polarized ω_s the SFG is small and is not explicitly considered here. Typical SFG spectra are shown in Fig. 3 for various ω_s and ω_i pulse fluences; with a linear polarizer placed at the entrance to the spectrometer, the SFG ω_s was determined to be p polarized to within experimental error. For the F1 spectrum both incident beams have a fluence of 80 μJ cm^{-2}; the resulting peak of the SFG response is at 795 nm and the spectral full width at half maximum (FWHM) is 9 nm. This contrasts with the SFG spectrum centered at 793 nm with a 17.5 nm FWHM, obtained from the convolution of the input ω_s and ω_i spectra (see Fig. 3). This difference is a consequence of the double-resonance coupling of the ω_i and ω_s beams to LEMs. An estimate of the enhancement relative to the unpatterned GaAs waveguide is obtained by moving the beams off the photonic crystal onto the surrounding wafer. The SFG response (expected to be s polarized) then vanishes and from the noise limitations it can be determined that the enhancement factor is $>350\times$. Also note that the input pulse spectra are wider than the LEMs to which they are coupled. Hence, a large portion of the incident pulses is not coupled to the PCW and is instead strongly reflected or scattered. Even though we have emphasized that this work is about the use of DFG and SFG as diagnostic tools, from previous second-harmonic experiments[5] we estimate the energy conversion in the DFG and SFG processes to be $<10^{-4}$. This can be improved upon by using structures with greater LEM Q factors than those obtained here.

Figure 3 also shows the effect of each pulse's fluence on the SFG spectrum. In the F2 spectrum the ω_s pulse fluence is 80 μJ cm^{-2} and that of the ω_i pulse is 400 μJ cm^{-2}; the fluences are exchanged to obtain the F3 spectrum. The F2 spectrum is essentially identical to the F1 spectrum, showing that SFG is not sensitive to either Kerr- or carrier-induced refractive index changes for high ω_i pulse fluence. In contrast, the F3 spectrum displays a small blueshift. From the fluence-dependent spectra the maximum amplitudes and wavelength shifts are extracted and shown in Figs. 4(a) and 4(b), respectively. The maximum amplitude of the SFG is plotted as a function of fluence for both the case where the ω_s fluence is fixed and the ω_i fluence is varied [F(1900), light circles] and vice versa [F(1360), dark circles]. In both cases the SFG intensity varies linearly with fluence. The peak position in the first case is unchanged as a function of increasing fluence (not shown). The wavelength shift $\Delta\lambda$ for the F(1360) case is given in Fig. 4(b). Over the range shown a linear dependence of the blueshift on fluence is observed with a maximum

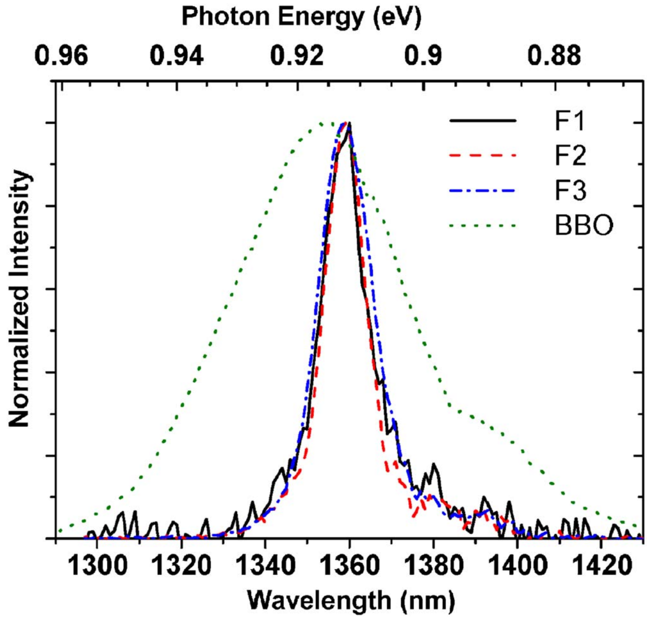

FIG. 5. (Color online) Normalized DFG spectra for the photonic crystal waveguide and BBO reference crystal. Various incident pulse fluences are indicated. For F1 both incident pulses have 80 μJ cm^{-2} fluence, for F2 the 793 nm pulse has a fluence of 80 μJ cm^{-2} with the 1900 nm pulse fluence being 400 μJ cm^{-2}. For F3 both incident pulses have 400 μJ cm^{-2} fluence.

shift[7,12] <1.5 nm. For the F(1360) case this linear dependence and the blueshift are indicative of single-photon absorption, most likely due to deep-center defects excited by the ω_s light.[13] This absorption leads to a very small refractive index change of the GaAs in the PCW ($\Delta n \simeq 0.006$ for F3).[14] The sharp spectral features in the SFG process make the observation of a small Δn possible.

Attempts to measure the photonic band structure with linear reflectivity in the 795 nm region to determine if any s- or p-polarized LEMs might contribute to the enhancement of p-polarized output were inconclusive. This is partially due to the absorption of the GaAs making reflectivity measurements extremely difficult because the Fano-like resonances are further broadened. However, since the GaAs is only 140 nm thick the SFG is still detectable. This is a further indication of the strength of the parametric conversion process as a diagnostic tool for PCWs.

IV. DIFFERENCE FREQUENCY GENERATION

For the DFG process the choice of p polarization for ω_p and s polarization for the ω_i beam maximizes the amplitude of the ω_s light so that the spectral and fluence-dependent characteristics can be determined. Attempts were made to measure DFG with both input beams s polarized but the DFG intensity was an order of magnitude smaller. For the DFG process emission at ω_s couples out via two orthogonally polarized LEMs. Figure 5 shows several normalized spectra from the PCW for different pulse fluences, as well as the DFG spectrum obtained from the BBO crystal. In spectrum F1, for which both pump beams have a fluence of 80 μJ cm^{-2}, the FWHM is 13.5 nm compared to 50 nm for the DFG from the BBO, which has no significant bandwidth restrictions. The spectral width of F1 is approximately four times smaller than the DFG spectrum from the BBO because of the resonance enhancement provided by the LEMs. Also, the FWHM of the DFG is larger than that in the SFG measurements. However, the effective Q factors (i.e., center wavelength/FWHM) of the two processes are $Q_{\mathrm{SFG}} \simeq 88$ and $Q_{\mathrm{DFG}} \simeq 109$, which are due to coupling to LEMs for both incoming and outgoing beams. Therefore, it is not surprising that a higher effective Q is obtained for the down conversion where (1) the generated light couples via LEMs and (2) the ω_p spectra at the nonresonant frequency are also narrow ($\sim$7.5 nm). The observed narrowing of the DFG ω_s from the PCW is associated with a $>500\times$ enhancement versus the surrounding bulk GaAs; this is greater than that obtained in SFG and is consistent with the effective Q factors. As for the SFG case, only part of the incident pulses' spectra can couple to the LEMs and contribute to the observed DFG, indicating that we again provide only a lower limit of the enhancement for the conversion process.

For the F2 spectrum the ω_i pulse fluence was raised to 400 μJ cm^{-2} (1360 nm pulse fluence is 80 μJ cm^{-2}), while for F3 both beam fluences were 400 μJ cm^{-2}. The center wavelengths and the line shapes of the three spectra appear to be identical within experimental uncertainty, indicating that the DFG process is not sensitive to either Kerr- or carrier-induced refractive index changes for the presented pump conditions. The lack of wavelength shift of the 1360 nm LEM is due to its being at a wavelength where the expected refractive index change induced by free-carrier excitation, band-gap shrinkage, and intraband contributions[12,15] is smallest ($|\Delta n| \leqslant 2\times 10^{-4}$).

The polarization properties of the DFG were studied with the 793 and 1900 nm pulse fluences equal to 160 and 320 μJ cm^{-2}, respectively. A zero-order quarter-wave plate was introduced into the 793 nm beam path to produce elliptically polarized light. If we denote by w the angle between the p-polarized 793 nm beam and the fast axis of the quarter-wave plate then $w=0$ or $\pm\pi/2$ correspond to p polarization while $w=\pm\pi/4$ correspond to right and left circularly polarized light. (Note that the polarizations inside the PCW are slightly different due to non-normal incidence of the excitation beams.) DFG spectra were obtained for $-\pi/2 \leqslant w \leqslant \pi/2$ in $\pi/12$ increments. From the spectra (not shown here), it is found that the center wavelength (1360 nm) does not vary significantly with w, although the line shape acquires a long-wavelength shoulder for ω_p beams which are not purely p polarized. More noticeably, there is a large change in the amplitude of the spectra as w varies respectively; the findings are summarized in Figs. 6 and 7. The fact that the intensities are different for right and left circularly polarized ω_p beams indicates that an s-polarized ω_p beam mixes with the s-polarized ω_i beam to produce a ω_s field that interferes with the ω_s field produced by the p-polarized ω_p mixing with the s-polarized ω_i beam. Indeed, this interference allows us to observe the presence of the former (s,s) mixing process, which is not easily observed alone, as noted above.

The polarization characteristics of the emitted DFG are shown in Fig. 6 for $w=0$, $\pi/4$, $-\pi/4$, and $-\pi/3$. In all cases the emission is linearly polarized to within experimental er-

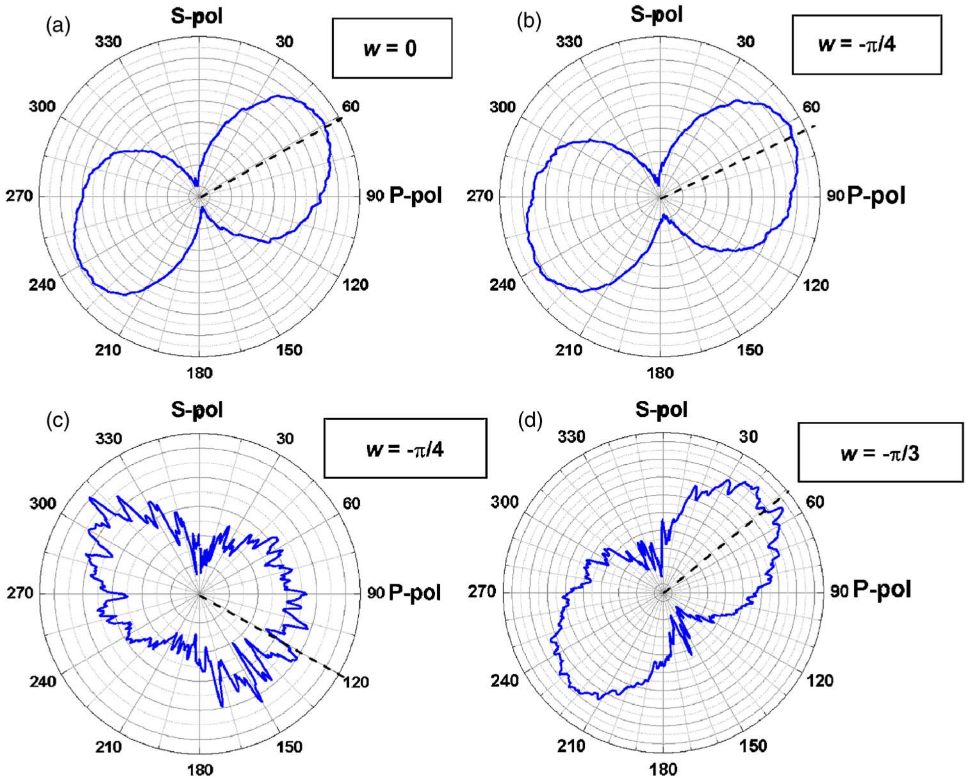

FIG. 6. (Color online) Dependence of DFG polarization from the photonic crystal as a function of the 793 nm pulse polarization: for four different values of wave-plate angle, w.

ror and has an associated polarization angle, α, which is measured relative to the s-polarization direction; for $w=0$ $\alpha=60°\pm8°$, as indicated by the dashed radial line in Fig. 6(a). Since there are two orthogonally polarized LEMs near 1360 nm, the induced second-order polarization density produces DFG light that is able to couple out via both modes. As w is varied, α is observed to vary dramatically, with the largest effect seen for $w=-\pi/4$ where $\alpha=120°\pm12°$, as seen in Fig. 6(c). A smaller rotation of the polarization plane occurs for $w=\pi/4$, as seen in Fig. 6(b). The overall dependence of α on w is summarized in Fig. 7(b).

The observed polarization and intensity characteristics can be understood quantitatively by considering the theory for parametric generation in the misoriented (relative to the electronic lattice) photonic crystal waveguide,[2] and indeed, might allow further detailed characteristics of LEMS to be determined. However, for this specific case, given that the PCW has various defects and imperfections, detailed calculations and comparisons with the data are impractical. Rather, in order to account for the main features of the data we begin with the knowledge that for an s-polarized ω_i beam and a p-polarized ω_p beam the DFG electric field, in relative units, is $\hat{s}+1.7\hat{p}$ where $\hat{s}$ and $\hat{p}$ denote unit vectors along the s- and p-polarized directions for the DFG beam. We then assume that an s-polarized ω_p beam mixing with the s-polarized ω_i beam would give a DFG field $a_s\exp(i\alpha_s)\hat{s}+a_p\exp(i\alpha_p)\hat{p}$, where a_s, α_s, a_p, and α_p are real constants. Therefore for arbitrary w, the p-polarized component of the DFG field is $1.7[\cos^2(w)+i\sin^2(w)]+a_p\exp(i\alpha_p)\cos(w)\sin(w)(1-i)$ while for the s component is $\cos^2(w)+i\sin^2(w)+a_s\exp(i\alpha_s)\cos(w)\sin(w)(1-i)$. From these expressions one can obtain the w dependence of the relative intensity and polarization plane orientation, which can be fitted to the DFG data. The curves shown in Fig. 7 are obtained for $a_s=1.1\pm0.05$, $\alpha_s=90°\pm10°$ with a_p being indistinguishable from zero (and its phase, α_p, indeterminate). Overall, the fit recovers the main features of the data includ-

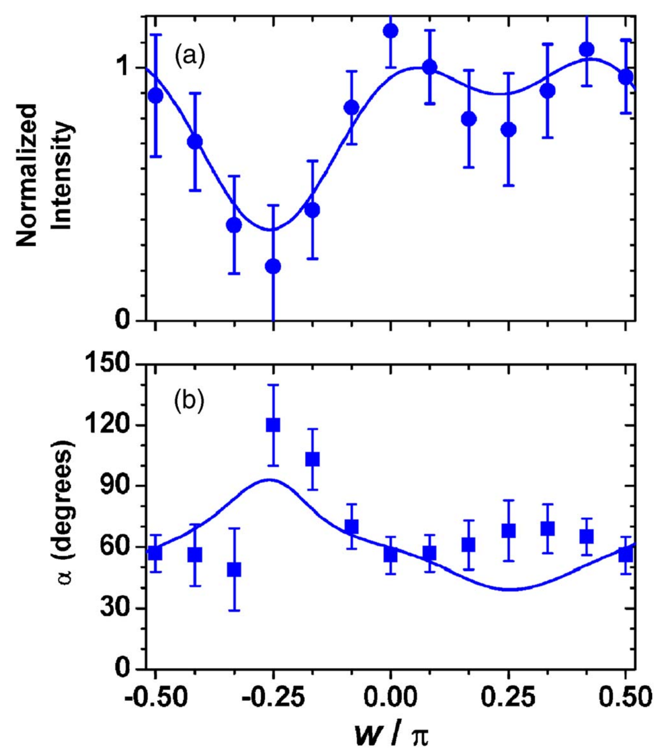

FIG. 7. (Color online) The experimental (points) and simulated (curves) for the DFG emission showing (a) the maximum intensity and (b) the polarization angle, α, as a function of wave-plate angle, w, associated with the 793 nm pulses.

ing the maintenance of linearly polarized DFG for all w. The only significant discrepancy occurs in the polarization plane orientation near $w=\pi/4$. Considering the error bars, the simplicity of the model, and sample imperfections, the overall agreement is good. Not only do these polarization studies allow us to access the DFG contribution from an s-polarized ω_p beam but also confirm that this contribution is much (four times) weaker in intensity than the contribution from the p-polarized ω_p beam. This simplified approach also gives us insight into the DFG polarization characteristics and accounts for the different amounts of polarization plane rotation for $w=\pm\pi/4$ as well as the associated intensity difference.

V. CONCLUSION

Sum and difference frequency generation have been observed in a 2D GaAs photonic crystal waveguide. Enhancements of at least 350× have been achieved by resonantly coupling to leaky eigenmodes for at least two of the three mixing fields. It is expected that for the same input fluence larger enhancements could be achieved by matching the bandwidth of the excitation beam to the Q factor of the coupling eigenmodes. Both processes show the strong spectral selectivity of resonant coupling in photonic crystal waveguides. In the sum frequency measurements, a subnanometer wavelength shift of the emission occurs and is explained in terms of small changes to the GaAs refractive index ($|\Delta n| \leq 0.006$) due to a strong 1360 nm pump beam. This is easily observed using parametric processes and would be difficult to discern using reflectivity techniques since the generated sum frequencies are above the electronic band gap of GaAs. The absorption leads to an amplitude change for the parametric process, whereas in reflectivity broadening of the Fano resonance would make it harder to elicit spectral information. Similarly, the observation of the large change in the difference frequency polarization are due to interference between strong and weak polarization components that would otherwise not be detectable; this sensitivity to the input fields demonstrates that the parametric conversion is a good diagnostic tool for the properties of the leaky eigenmodes.

Further extensions can be explored, such as other angles of incidence and noncollinear geometries to spectroscopically study the leaky eigenmodes; this could be especially useful with alternative intense light sources, e.g., laser supercontinuums. In addition to the spectroscopic versatility, the demonstration of down conversion in photonic crystals also opens up the possibility of producing entangled photons,[16] especially from points in the band structure where degenerate orthogonally polarized eigenmodes occur.

ACKNOWLEDGMENTS

The authors would like to acknowledge A. R. Cowan, W. Jiang, and Jeff F. Young for design and fabrication of the sample, as well as continued fruitful discussion. This work was funded by the Natural Sciences and Engineering Research Council of Canada and Photonics Research Ontario.

[1] T. F. Krauss, R. M. De La Rue, and S. Brand, Nature (London) **383**, 699 (1986).
[2] A. R. Cowan and J. F. Young, Phys. Rev. B **65**, 085106 (2002).
[3] L. C. Andreani *et al.*, Physica E (Amsterdam) **17**, 402 (2003).
[4] A. M. Malvezzi *et al.*, Phys. Rev. B **68**, 161306R (2003).
[5] J. P. Mondia, H. M. van Driel, W. Jiang, A. R. Cowan, and J. F. Young, Opt. Lett. **28**, 2500 (2003).
[6] V. N. Astratov, I. S. Culshaw, R. M. Stevenson, D. M. Whittaker, M. S. Skolnick, T. F. Krauss, and R. M. De La Rue, J. Lightwave Technol. **17**, 2050 (1999).
[7] A. D. Bristow *et al.*, Appl. Phys. Lett. **83**, 851 (2003).
[8] U. Fano, Phys. Rev. **124**, 1866 (1961).
[9] P. P. Markowicz, H. Tiryaki, H. Pudavar, P. N. Prasad, N. L. Lepeshkin, and R. W. Boyd, Phys. Rev. Lett. **92**, 083903 (2004).
[10] K. Sakoda and K. Ohtaka, Phys. Rev. B **54**, 5742 (1996).
[11] *Handbook of Optical Constants in Solids*, edited by E. D. Palik (Academic, New York, 1985).
[12] J. P. Mondia, H. W. Tan, S. Linden, H. M. van Driel, and J. F. Young, J. Opt. Soc. Am. B **22**, 2480 (2005).
[13] This is verified by nonlinear pump-probe spectroscopy (see Ref. 12) and independently by stimulated Raman-scattering experiments, J. F. Young (private communication).
[14] The change of refractive index can be estimated from the wavelength shift (Ref. 7) for a particular fluence by the relationship $\Delta n \simeq \Delta\lambda n_{\mathrm{eff}}/\lambda$, where $n_{\mathrm{eff}} \simeq 3.65$ at $\lambda=795$ nm.
[15] B. R. Bennett, R. A. Soref, and J. A. Del Alamo, IEEE J. Quantum Electron. **26**, 113 (1990).
[16] M. J. A. de Dood, W. T. M. Irvine, and D. Bouwmeester, Phys. Rev. Lett. **93**, 040504 (2004).